

Efficient and Accurate Linear Algebraic Methods for Large-scale Electronic Structure Calculations with Non-orthogonal Atomic Orbitals

H. Teng^{1,*}, T. Fujiwara^{1,2,†}, T. Hoshi^{3,2}, T. Sogabe^{4,2}, S.-L. Zhang^{5,2}, and S. Yamamoto^{6,2}

(1) *Center for Research and Development of Higher Education,
The University of Tokyo, Bunkyo-ku, Tokyo, 113-8656, Japan*

(2) *Core Research for Evolutional Science and Technology,
Japan Science and Technology Agency (CREST-JST), Japan*

(3) *Department of Applied Mathematics and Physics, Tottori University, Tottori 680-8550, Japan*

(4) *School of Information Science and Technology,
Aichi Prefecture University, Nagakute-cho, Aichi 480-1198, Japan*

(5) *Department of Computational Science and Engineering,
Nagoya University, Chikusa-ku, Nagoya 464-8603, Japan and*

(6) *School of Computer Science, Tokyo University of Technology,
Katakura-machi, Hachioji, Tokyo 192-0982, Japan*

(Dated: May 29, 2018)

The need for large-scale electronic structure calculations arises recently in the field of material physics and efficient and accurate algebraic methods for large simultaneous linear equations become greatly important. We investigate the generalized shifted conjugate orthogonal conjugate gradient method, the generalized Lanczos method and the generalized Arnoldi method. They are the solver methods of large simultaneous linear equations of one-electron Schrödinger equation and maps the whole Hilbert space to a small subspace called the Krylov subspace. These methods are applied to systems of fcc Au with the NRL tight-binding Hamiltonian (Phys. Rev. B **63**, 195101 (2001)). We compare results by these methods and the exact calculation and show them equally accurate. The system size dependence of the CPU time is also discussed. The generalized Lanczos method and the generalized Arnoldi method are the most suitable for the large-scale molecular dynamics simulations from the view point of CPU time and memory size.

PACS numbers: 71.15.-m, 02.70.Ns, 71.15.Pd

I. INTRODUCTION

In recent years, molecular dynamics (MD) simulations with electronic structure calculations in nano-scale structures have attracted much attention. One needs a large size of systems of several hundred thousands atoms with a few hundred pico-seconds (or more longer time) process in order to investigate characteristics of nano-scale systems such as phenomena of competition between different physical principles or phenomena of the multi-physics, e.g. energy competition between the strain field and chemical bonds.¹⁻⁴ Several requirements for large-scale MD simulation with electronic structure calculations are contradictory to each other, e.g. total energy accuracy *vs.* larger system size or longer physical time of processes.

There are several approaches for large-scale MD simulations;⁵ (a) the Fermi operator expansion,⁶ (b) the divide-and-conquer method,⁷ and (c) the minimization method (the density matrix minimization⁸ or the wavefunction minimization⁹). Another classification may be the one according as the basis set of wavefunctions; (a) the plane wave basis set and switching between the real-space and k -space representation,¹⁰ and (b) localized orbitals¹¹ or tight-binding basis set.¹² Computation with “massively parallel machine” is also an important issue.

An important aspect is development of novel algebraic algorithm for extra-large scale systems. The most general and important algorithm may be the linear algebra

solving simultaneous linear equations

$$(z - H)\mathbf{x} = \mathbf{b}, \quad (1)$$

where H is self-adjoint or real symmetric matrix, \mathbf{b} is a given vector, $z = \varepsilon + i\eta$, ε is an energy parameter and η is an infinitesimally small positive number, respectively. Solutions of Eq.(1) relate to the standard eigenvalue problem $(\varepsilon - H)\mathbf{x} = 0$. We developed the subspace diagonalization method and the shifted conjugate orthogonal conjugate gradient (COCG) method.¹³⁻¹⁶ Then the methods were applied to the fracture propagation and surface formation in Si crystals with the tight-binding Hamiltonian based on an orthogonal basis set.^{1,2} On the other hand, since its Hamiltonian is described by the tight-binding Hamiltonian based on a non-orthogonal basis set, the problem of the formation of Au multishell helical nanowires was solved by the exact diagonalization method.^{3,4}

Development of efficient linear algebraic methods has been, so far, mainly based on the orthogonal basis sets.^{13,14,17-19} However, localized basis wavefunctions are generally non-orthogonal and it is much desirable to generalize the methods to the case of a non-orthogonal basis set. The most popular strategy of the generalized eigenvalue problem (represented by the non-orthogonal basis set) would be the transformation to the standard eigenvalue problem.¹⁹ Our target in the present paper is to solve simultaneous linear equations with self-adjoint or

real symmetric matrix S ;

$$(zS - H)\mathbf{x} = \mathbf{b}, \quad (2)$$

which relates to the generalized eigen-value problem $(\varepsilon S - H)\mathbf{x} = 0$. We will investigate efficient methods of solving Eq.(2) with a complex energy variable z when the matrix size of H and S is huge. Several algebraic algorithms will be discussed and directly applied to a tight-binding Hamiltonian based on non-orthogonal atomic orbitals in large-scale systems.

The structure of the present paper is as follows. In Section II, the idea of non-orthogonal atomic orbitals and physical properties (e.g. the band energy, the local/partial density of states, numbers of occupied electron states, the chemical potential *et al.*) are summarized. Sections III, IV and V explain three different algorithms of large-scale linear equations, *i.e.* the generalized shifted conjugate orthogonal conjugate gradient method (GsCOCG), the generalized Lanczos method and the generalized Arnoldi method which generate the Krylov subspace from the whole Hilbert space. In these sections, numerical examples are presented by using the NRL tight-binding Hamiltonian. The generalized Lanczos method becomes applicable to actual large systems with a high accuracy if one use the modified Gram-Schmidt reorthogonalization to maintain the orthogonality of generated basis vectors. In Section VI, we compare the CPU-times of each algorithm and discuss the applicability to large-scale electronic structure calculations and MD simulations. Section VII is conclusions. The examples without reorthogonalization in the generalized Lanczos method are shown and discussed in Appendix A. Appendix B is devoted to discuss the consistency between the total energy and force.

II. THEORETICAL BACKGROUND

A. Non-orthogonal basis set and S-orthogonalization

We define two sets of wavefunctions, $\{\phi_i(\mathbf{r})\}$ and $\{\psi_\alpha(\mathbf{r})\}$, where $\{\phi_i(\mathbf{r})\}$ is the non-orthogonal (normalized) basis set (e.g. atomic orbitals and ‘ i ’ denotes an atomic site and energy level), and $\{\psi_\alpha(\mathbf{r})\}$ is the orthonormalized basis set. Then the overlap matrix S_{ij} and the Hamiltonian matrix H_{ij} are defined as

$$S_{ij} = \langle \phi_i | \phi_j \rangle = \int \phi_i^* \phi_j d\mathbf{r}, \quad S_{ii} = 1, \quad (3)$$

$$H_{ij} = \langle \phi_i | \hat{H} | \phi_j \rangle = \int \phi_i^* \hat{H} \phi_j d\mathbf{r}, \quad (4)$$

where \hat{H} is the Hamiltonian operator. The orthonormal basis set $\{\psi_\alpha(\mathbf{r})\}$ can be expanded in terms of $\{\phi_j\}$ as

$$\psi_\alpha(\mathbf{r}) = \sum_i \phi_i(\mathbf{r}) w_i^{(\alpha)} \quad (5)$$

and the orthogonality relation is expressed as

$$\langle \psi_\alpha | \psi_\beta \rangle = \sum_{ij} w_i^{(\alpha)*} w_j^{(\beta)} S_{ij} \quad (6)$$

$$\equiv (\mathbf{w}^{(\alpha)}, \mathbf{w}^{(\beta)})_S = \delta_{\alpha\beta}, \quad (7)$$

where $\mathbf{w}^{(\alpha)} = (w_1^{(\alpha)}, w_2^{(\alpha)}, \dots)^t$. We call the representation $(\mathbf{w}^{(\alpha)}, \mathbf{w}^{(\beta)})_S$ the ‘‘S-product’’ and the relation Eq. (7) the ‘‘S-orthogonalization’’ of basis vectors $\mathbf{w}^{(\alpha)}$.

When $\psi_\alpha(\mathbf{r})$ satisfies the Schrödinger equation

$$\hat{H}\psi_\alpha(\mathbf{r}) = \varepsilon_\alpha \psi_\alpha(\mathbf{r}), \quad (8)$$

coefficients $\{w_i^{(\alpha)}\}$ should be elements of an eigen-vector of a simultaneous linear equation in the ϕ -representation;

$$\sum_i H_{ji} w_i^{(\alpha)} = \varepsilon_\alpha \sum_i S_{ji} w_i^{(\alpha)} \quad (9)$$

or, in matrix-vector form,

$$H\mathbf{w}^{(\alpha)} = \varepsilon_\alpha S\mathbf{w}^{(\alpha)}. \quad (10)$$

Matrices $H = (H_{ij})$ and $S = (S_{ij})$ are self-adjoint in ϕ -representation.

B. Green’s function and local/partial density of states represented by the non-orthogonal basis set

The Green’s operator \hat{G} is defined as

$$\hat{G}(z) = \{(\varepsilon + i\eta)\hat{1} - \hat{H}\}^{-1}, \quad (11)$$

where $\hat{1}$ is the identity operator and $z = \varepsilon + i\eta$. Elements of the Green’s function matrix can, then, be written as

$$G_{ij}(z) = \langle \phi_i | \hat{G}(z) | \phi_j \rangle = \{S(zS - H)^{-1}S\}_{ij} \quad (12)$$

$$= \sum_{k,l} S_{ik} \left\{ \sum_{\alpha} w_k^{\alpha*} \frac{1}{z - \varepsilon_\alpha} w_l^{\alpha} \right\} S_{lj}. \quad (13)$$

The local (partial) densities of states is expressed in the ϕ -representation as follows:

$$D_{ij}(\varepsilon) = -\frac{1}{\pi} \text{Im}(G(z)S^{-1})_{ij}. \quad (14)$$

The normalization of the Green’s functions and the local/partial density of states (DOS) is then

$$\left(-\frac{1}{\pi}\right) \int_{-\infty}^{\infty} d\varepsilon \text{Im}G_{ij}(z) = \langle \phi_i | \phi_j \rangle = S_{ij}, \quad (15)$$

$$\int_{-\infty}^{\infty} d\varepsilon D_{ii}(\varepsilon) = 1. \quad (16)$$

C. Total band energy and Green's function

1. Density matrix and energy density matrix

In the simulation process, the density matrix ρ_{ij} and the energy density matrix π_{ij} appear repeatedly in the calculation of the Mulliken charge, the total energy and forces,²⁰ whose definition may be

$$\rho_{ij} = \left(-\frac{1}{\pi}\right) \text{Im} \int d\varepsilon \sum_{\alpha} f(\varepsilon_{\alpha}) \frac{w_i^{(\alpha)*} w_j^{(\alpha)}}{z - \varepsilon_{\alpha}} \quad (17)$$

$$= \sum_{\alpha} f(\varepsilon_{\alpha}) w_i^{(\alpha)*} w_j^{(\alpha)}, \quad (18)$$

$$\pi_{ij} = \left(-\frac{1}{\pi}\right) \text{Im} \int d\varepsilon \varepsilon \sum_{\alpha} f(\varepsilon_{\alpha}) \frac{w_i^{(\alpha)*} w_j^{(\alpha)}}{z - \varepsilon_{\alpha}} \quad (19)$$

$$= \sum_{\alpha} f(\varepsilon_{\alpha}) \varepsilon_{\alpha} w_i^{(\alpha)*} w_j^{(\alpha)}, \quad (20)$$

where $f(\varepsilon)$ is the Fermi-Dirac function $f(\varepsilon) = \{1 + \exp((\varepsilon - \mu)/\tau)\}^{-1}$, where μ and τ are the chemical potential and temperature.

2. Physical property

The chemical potential μ should be determined by the equation for the total electron number N_{tot} :

$$N_{\text{tot}} = 2 \sum_i \int d\varepsilon f(\varepsilon) D_{ii}(\varepsilon) \quad (21)$$

$$= \sum_{ij\alpha} S_{ij} \left(-\frac{2}{\pi}\right) \text{Im} \int d\varepsilon f(\varepsilon_{\alpha}) \frac{w_j^{(\alpha)*} w_i^{(\alpha)}}{z - \varepsilon_{\alpha}} \quad (22)$$

$$= 2 \sum_{ij} S_{ij} \rho_{ji}, \quad (23)$$

where a factor “2” is the spin degeneracy.

The total band energy of the system is given as

$$E_{\text{tot}} = 2 \sum_{\alpha}^{\text{occ}} \varepsilon_{\alpha} = 2 \sum_{\alpha} \varepsilon_{\alpha} f(\varepsilon_{\alpha}) \quad (24)$$

$$= -\frac{2}{\pi} \text{Im} \sum_i \int d\varepsilon \varepsilon f(\varepsilon) (G(z)S^{-1})_{ii}, \quad (25)$$

where the summation $\sum_{\alpha}^{\text{occ}}$ runs over the occupied states. This equation can be expressed by the density of states, the density matrix or the energy density matrix as

$$E_{\text{tot}} = 2 \sum_i \int d\varepsilon \varepsilon f(\varepsilon) D_{ii}(\varepsilon) \quad (26)$$

$$= 2 \sum_{ij} \rho_{ij} H_{ji} \quad (27)$$

$$= 2 \sum_{ij} S_{ij} \pi_{ji}. \quad (28)$$

Moreover, any physical property can be expressed by using the density matrix as

$$\begin{aligned} \langle X \rangle &= \left(-\frac{2}{\pi}\right) \int d\varepsilon f(\varepsilon) \sum_{ij} X_{ij} \text{Im}(S^{-1}G(z)S^{-1})_{ji} \\ &= 2 \sum_{ij} X_{ij} \rho_{ji}. \end{aligned} \quad (29)$$

The expressions Eqs. (27) and (28) and also (29) are satisfied not only in the whole Hilbert space but also in the mapped subspace in which we construct approximate eigen-states.

Now we have obtained three different expressions Eqs.(21)~(23) for N_{tot} and Eqs.(26)~(28) for E_{tot} . These expressions normally give different values, because we usually use finite values of the energy interval, η and approximate eigen-states in the mapped subspace. Fortunately, if the formula $\sum_{ij} \rho_{ij} H_{ji} = \sum_{ij} S_{ij} \pi_{ji}$ is satisfied, the consistency between the total band energy and the force can be kept as shown in Appendix B.

III. GENERALIZED SHIFTED COCG METHOD

We developed the shifted COCG method for large-scale linear equations (1).^{14,15,21} It was shown that the convergence behavior can be monitored by observing the behavior of the “residual norm”. The shifted COCG method is generalized for Eq.(2) in this section.

A. Definition of the problem

The eigen-value problem of stationary Schrödinger equation is equivalent to the scattering problem;

$$(z\hat{1} - \hat{H})\psi(\mathbf{r}) = \chi(\mathbf{r}), \quad (30)$$

where $z = \varepsilon + i\eta$ and ε is an energy parameter of incident waves. The wavefunction $\psi(\mathbf{r})$ is expanded by the set of non-orthogonal atomic orbitals $\{\phi_j\}$;

$$\psi(\mathbf{r}) = \sum_j \phi_j(\mathbf{r}) x_j(z). \quad (31)$$

Substituting Eq. (31) into Eq. (30), one obtains generalized linear equations

$$(zS - H)\mathbf{x}(z) = \mathbf{b}, \quad (32)$$

where the j -th component of the vector \mathbf{b} is $b_j = \langle \phi_j | \chi \rangle$. The solution of the linear equation $\mathbf{x}(z)$ is then

$$\mathbf{x}(z) = (zS - H)^{-1} \mathbf{b} = S^{-1}G(z)S^{-1} \mathbf{b} \quad (33)$$

with a help of Eq. (12). By setting a vector \mathbf{b} as

$$\mathbf{b} = \mathbf{e}_j = (0, 0, \dots, 0, \underbrace{1}_j, 0, 0, \dots)^t, \quad (34)$$

we can get the corresponding solution $\mathbf{x}^j(z)$ as

$$\mathbf{x}^j(z) = S^{-1}G(z)S^{-1}\mathbf{e}_j. \quad (35)$$

The product of \mathbf{e}_i and \mathbf{x}^j (not S-product), the i -th element of a vector \mathbf{x}^j , is identical just to the energy-component of the density matrix $\rho_{ij}(\varepsilon)$;

$$\rho_{ij}(\varepsilon) = -\frac{1}{\pi}\text{Im}\left[\mathbf{e}_i^t \cdot \mathbf{x}^j(\varepsilon + i\eta)\right], \quad (36)$$

which relates to the local DOS as

$$D_{ii}(\varepsilon) = \sum_k S_{ik}\rho_{ki}(\varepsilon). \quad (37)$$

Then the density matrix and the energy density matrix are given by the integrations of $\rho_{ij}(\varepsilon)$ as

$$\rho_{ij} = \int d\varepsilon f(\varepsilon)\rho_{ij}(\varepsilon), \quad (38)$$

$$\pi_{ij} = \int d\varepsilon \varepsilon f(\varepsilon)\rho_{ij}(\varepsilon). \quad (39)$$

It should be noticed here that there is no quantities of eigen-energies in the Krylov subspace and, we should use the calculation procedure through $\rho_{ij}(\varepsilon)$ rather than the calculation of Eqs.(18) and (20). Their resultant values depend on the interval of energy mesh-points for the energy integration and a fictitious finite value of η .

B. Generalized shifted conjugate orthogonal conjugate gradient (GsCOCG) method

For non-orthogonal basis set, we can generalize the shifted COCG procedure, named the generalized shifted COCG (GsCOCG) method.²² The linear equations of the ‘seed’ energy σ_s and the ‘shift’ energy σ , respectively, are written down as

$$(S^{-1}A + \sigma_s \mathbf{1})\mathbf{x} = S^{-1}\mathbf{b}, \quad (40)$$

$$(S^{-1}A + \sigma \mathbf{1})\mathbf{x}^{(i)} = S^{-1}\mathbf{b}, \quad (41)$$

where the matrix A is defined as

$$A = z_{\text{ref}}S - H \quad (42)$$

with an arbitrary reference energy $z_{\text{ref}} = \varepsilon_{\text{ref}} + i\eta$, $\mathbf{1}$ is the unit matrix and $\mathbf{b} = \mathbf{e}_j$. The seed energy and the ‘shift energy’ are given as $\varepsilon_s = \varepsilon_{\text{ref}} + \sigma_s$ and $\varepsilon = \varepsilon_{\text{ref}} + \sigma$.

Following the procedure of the shifted COCG method,^{15,16} we try to find iterative n -th solutions \mathbf{x}_n in the Krylov subspace defined

$$\begin{aligned} & K_n(S^{-1}A + \sigma_s \mathbf{1}, S^{-1}\mathbf{b}) \\ & = \text{Span}\{S^{-1}\mathbf{b}, S^{-1}AS^{-1}\mathbf{b}, (S^{-1}A)^2S^{-1}\mathbf{b}, \\ & \quad \dots, (S^{-1}A)^n S^{-1}\mathbf{b}\}. \end{aligned} \quad (43)$$

This yields the residual vector $\mathbf{r}'_n = S^{-1}\mathbf{b} - (S^{-1}A + \sigma_s \mathbf{1})\mathbf{x}_n$ to be²²

$$\mathbf{r}'_n \perp K_n((S^{-1}A + \sigma_s \mathbf{1})^\dagger, \mathbf{b}^*), \quad (44)$$

where B^\dagger is the Hermitian conjugate matrix of B and \mathbf{b}^* is the complex conjugate vector of \mathbf{b} . The actual algorithms may be as follows. Under the initial conditions

$$\mathbf{x}_0 = \mathbf{p}_{-1} = \mathbf{0}, \quad (45)$$

$$\mathbf{r}_0 = \mathbf{b}, \quad (46)$$

$$\alpha_{-1} = 1, \quad \beta_{-1} = 0, \quad (47)$$

and a definition $\mathbf{r}'_0 = S^{-1}\mathbf{r}_0$, we evaluate the following equations for the ‘seed’ energy σ_s iteratively for $n = 0, 1, 2, \dots$:

$$\begin{aligned} \mathbf{p}_n &= \mathbf{r}'_n + \beta_{n-1}\mathbf{p}_{n-1}, \\ \alpha_n &= \frac{(\mathbf{r}'_n, \mathbf{r}'_n)_S}{(\mathbf{p}_n, S^{-1}(A + \sigma_s S)\mathbf{p}_n)_S}, \\ \mathbf{x}_{n+1} &= \mathbf{x}_n + \alpha_n \mathbf{p}_n, \\ \mathbf{r}_{n+1} &= \mathbf{r}_n - \alpha_n (A + \sigma_s S)\mathbf{p}_n, \\ \mathbf{r}'_{n+1} &= S^{-1}\mathbf{r}_{n+1}, \\ \beta_n &= \frac{(\mathbf{r}'_{n+1}, \mathbf{r}'_{n+1})_S}{(\mathbf{r}'_n, \mathbf{r}'_n)_S}. \end{aligned} \quad (48)$$

Important point here is our use of $\mathbf{r}'_n = S^{-1}\mathbf{r}_n$. In actual procedure, we employ a form $\mathbf{r}_n = S\mathbf{r}'_n$ at each iteration step by CG method. Since the overlap matrix S is real symmetric positive definite and sparse, the convergence of CG iteration can be fast.

The basic theorem of the Krylov subspace is the invariance of the subspace under an energy shift σ . The other very basic theorem is the *collinear residual*²³

$$\mathbf{r}_n^\sigma = \frac{1}{\pi_n^\sigma} \mathbf{r}_n. \quad (49)$$

Owing to these theorems, once we solve the set of equations for the ‘seed’ energy σ_s , we can obtain the results for any shift energy σ only by scalar multiplications. The recurrence equations for shift energies are given (all the quantities are denoted by the superscript σ), with initial values $\pi_{-1}^\sigma = \pi_0^\sigma = 1$, as follows;

$$\pi_{n+1}^\sigma = \left\{1 + \alpha_n(\sigma - \sigma_s)\right\} \pi_n^\sigma + \frac{\beta_{n-1}}{\alpha_{n-1}} \alpha_n (\pi_n^\sigma - \pi_{n-1}^\sigma) \quad (50)$$

and

$$\mathbf{x}_{n+1}^\sigma = \mathbf{x}_n^\sigma + \alpha_n^\sigma \mathbf{p}_n^\sigma \quad (51)$$

with

$$\begin{aligned} \alpha_n^\sigma &= \frac{\pi_n^\sigma}{\pi_{n+1}^\sigma} \alpha_n, \\ \beta_{n-1}^\sigma &= \left(\frac{\pi_{n-1}^\sigma}{\pi_n^\sigma}\right)^2 \beta_{n-1}, \\ \mathbf{p}_n^\sigma &= \frac{1}{\pi_n^\sigma} \mathbf{r}'_n + \beta_{n-1}^\sigma \mathbf{p}_{n-1}^\sigma. \end{aligned}$$

Partial densities of states are shown in Fig. 1 for a system of Au 864 atoms by NRL tight-binding Hamiltonian,²⁴ in comparison with those by the exact calculations. In order to see the behavior of the peak positions and the tail of the peaks, the figures are drawn in the logarithmic scale. Two lines of GsCOCG and the exact calculation overlap each other almost completely and one can recognize an excellent agreement between the two different calculations.

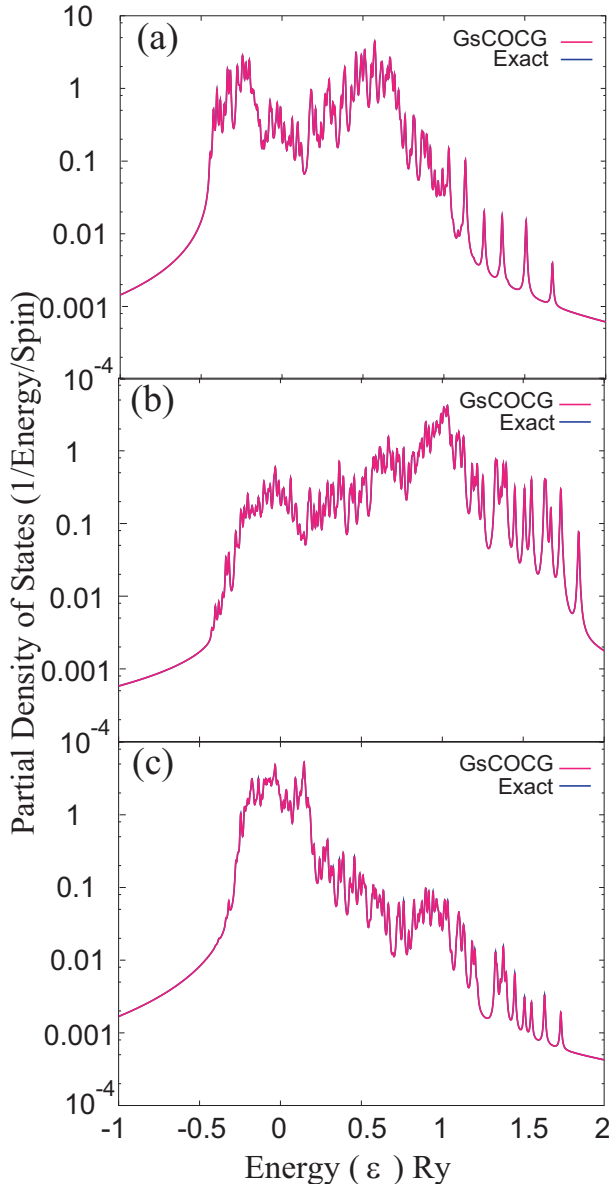


FIG. 1: (Color on line) Partial density of states for a system of Au 864 atoms by NRL tight-binding Hamiltonian,²⁴ normalized to unity. (a) s-orbitals, (b) p-orbitals and (c) d-orbitals. Comparison is for GsCOCG and the exact calculation, which are almost identical to each other. Parameters in GsCOCG calculations are $\eta = 10^{-3}\text{Ry}$, $\tau = 5\eta$. The energy interval of mesh-points is 10^{-4}Ry . See Figs. 4, 5 and 7 for comparison.

C. Residual norm and convergence behavior

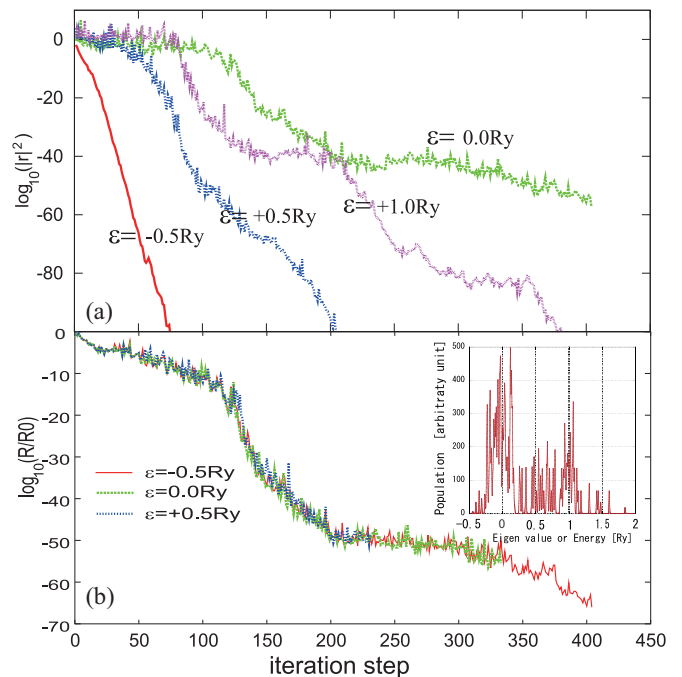


FIG. 2: (Color on line) Convergence behavior of residual norms for a system of Au 256 atoms by NRL tight-binding Hamiltonian.²⁴ Spectrum extends between -0.5 Ry to 1.5 Ry . The inset in (b) show the total density of states $D(\varepsilon) = \sum_i D_{ii}(\varepsilon)$, where we use a finite imaginary number in the energy and the profile is of dense spiky peaks. (a) Residual norm $\|\mathbf{r}_n^{(s,j)}\|$ at several energy points $\varepsilon = -0.5, 0.0, 0.5, 1.0\text{ Ry}$ for s-orbital. (b) Average residual norms $R_n^{(j)}$ with different three seed energies ($-0.5, 0.0, 0.5\text{ Ry}$) for s-orbital and they all overlap with each other.

The useful characteristic property of GsCOCG method is the capability of monitoring the norm of residual vectors.¹⁴ The residual vectors for the seed and shift equations with an energy ε_k (with $\mathbf{b} = \mathbf{e}_j$ and $\sigma_k = \varepsilon_k - \varepsilon_{\text{ref}}$) are $\mathbf{r}_n^{(s,j)}$ and $\mathbf{r}_n^{(k,j)}$, respectively, and the ‘mapped’ residual vectors for the seed and shift equations $\mathbf{r}_n^{\prime(s,j)} = S^{-1}\mathbf{r}_n^{(s,j)}$ and $\mathbf{r}_n^{\prime(k,j)} = S^{-1}\mathbf{r}_n^{(k,j)}$. We usually need only elements of the density matrix among near-sited orbital pairs connected by non-zero elements of the Hamiltonian or overlap matrices and the convergence monitoring is necessary for these components.¹⁴ Therefore, in order to monitor the convergence behavior, we adopt the “residual norm” defined as

$$\|\mathbf{r}_n^{\prime(s/k,j)}\|^2 \equiv \sum_i^{H_{ij} \neq 0} |\mathbf{e}_i^t \cdot \mathbf{r}_n^{\prime(s/k,j)}|^2. \quad (52)$$

Furthermore, since the residual norm is different among different energy points, the average quantity (“average

residual norm”) should be defined as¹⁴

$$\begin{aligned} R_n^{(j)} &\equiv \frac{1}{N_{\text{ene}}} \sum_k^{N_{\text{ene}}} \|\mathbf{r}_n^{(k,j)}\|^2 \\ &= \|\mathbf{r}_n^{(s,j)}\|^2 \frac{1}{N_{\text{ene}}} \sum_k^{N_{\text{ene}}} \frac{1}{|\pi_k|^2}, \end{aligned} \quad (53)$$

where N_{ene} is the number of energy points.

The convergence behavior of the residual norm for different seed energies is shown in Fig. 2a. The convergence at the energy of the low DOS is very fast, because the eigen-state can be constructed by a small number of basis states. The convergence of the averaged norm is shown in Fig. 2b, which confirms numerically the fact that the average residual norm (and all the physical quantities) does not depend sensitively on the choice of a seed energy.

D. Seed-switching technique

When one chooses a seed energy in an energy range of rapid convergence, the spectra at majority energy points have not been converged yet and one should restart the calculation with a new seed energy as seen in Fig. 2a. The most desirable seed energy may be the one of the largest (partial) DOS because the convergence at these point is the most slowest.

However, even if one chooses a starting seed energy in the highest DOS region and the residual norm at the seed energy reaches the convergence criterion, it often happens that there still remain several energy points/regions where the residual norm has not been small enough. Fortunately the shifting energy does not need any additional heavy computational task but several scalar manipulation as Eq.(50). Because of this property of shifting energy, a choice of a seed energy σ_s can be arbitrary. As shown in Fig.2b, even if we start with an improper seed energy and switch a seed, the total iteration times for desired convergence over whole energy range is not very different. The *seed-switching* is very efficient technique to avoid restarting the calculation from the beginning with a new seed energy.^{16,25} One chooses a new seed energy σ_s^{new} and can continue the calculation without discarding the information of the previous calculation with the old σ_s by using the shift property. Figure 3 shows the behavior of the residual norms in the seed-switching process.

IV. GENERALIZED LANCZOS PROCESS AND DENSITY OF STATES

The three-term recursive relation used in GsCOCG method leads us to the generalization of the Lanczos method.^{18,19,26} As far as we know, the generalization of the Lanczos method was presented first in Ref. 18. In this section, we will stress that the generalized Gram-Schmidt reorthogonalization process makes G-Lanczos

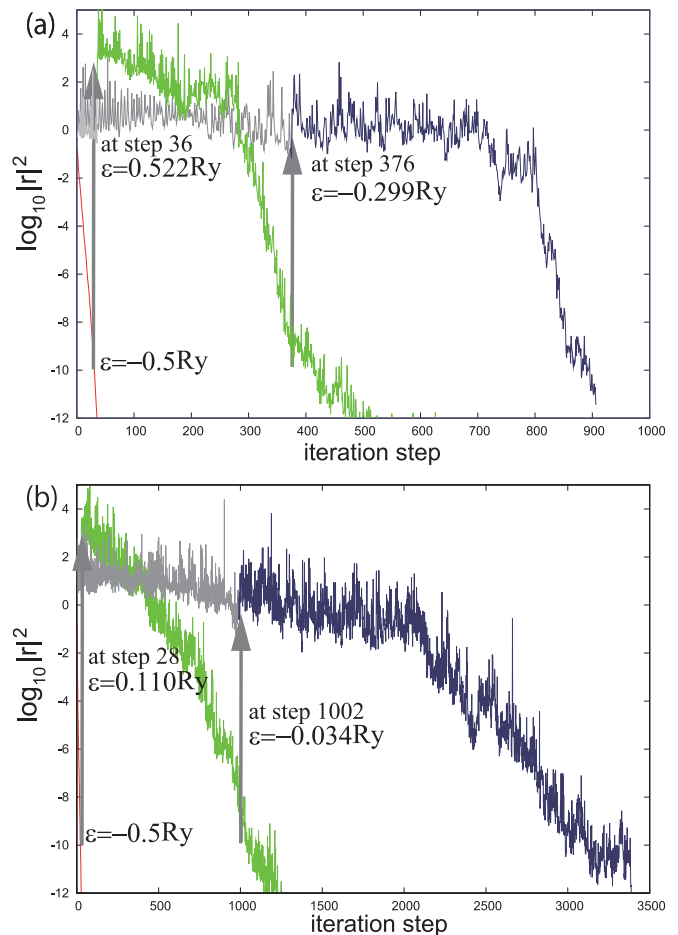


FIG. 3: (Color on line) Residual norm at the seed energies for a system of Au 864 atoms by the NRL tight-binding Hamiltonian,²⁴ in s-orbitals (a) and d-orbitals (b). (a) Seed-switches to 0.0 Ry from -0.5 Ry at 36-th step and to -0.299 Ry at 376-th step in the s-orbital case. (b) Seed-switches to 0.110 Ry from -0.5 Ry at 28-th step and to -0.034 Ry at 1002-nd step in the d-orbital case. Once the calculation using one seed is converged and full convergence has not been achieved, one should choose the next seed and continue the calculation. The gray lines show the residual norm by energy shift \mathbf{r}_n^σ before seed-switching.

method practically useful and also the use of Eqs.(18) and (20) gives very efficient and accurate results.

A. Generalized Lanczos process

First we define a matrix \mathcal{H} as

$$\mathcal{H} \equiv S^{-1}H, \quad (54)$$

which is not self-adjoint but still satisfies the *quasi-Hermitian* property in the S-product;

$$(\mathbf{v}, \mathcal{H}\mathbf{u})_S = (\mathcal{H}\mathbf{v}, \mathbf{u})_S. \quad (55)$$

We can construct the three-term procedure of the Lanczos process ($n = 0, 1 \dots$) as^{18,19}

$$\mathcal{H}\mathbf{u}^n = a_n\mathbf{u}^n + b_{n+1}\mathbf{u}^{n+1} + b_n\mathbf{u}^{n-1}, \quad (56)$$

where

$$\begin{aligned} a_n &= (\mathbf{u}^n, \mathcal{H}\mathbf{u}^n)_S, \\ b_{n+1}^2 &= ((\mathcal{H} - a_n)\mathbf{u}^n - b_n\mathbf{u}^{n-1}, (\mathcal{H} - a_n)\mathbf{u}^n - b_n\mathbf{u}^{n-1})_S, \\ \mathbf{u}^{n+1} &= \{(\mathcal{H} - a_n)\mathbf{u}^n - b_n\mathbf{u}^{n-1}\}/b_{n+1} \end{aligned}$$

with conditions $b_0 = 0$, $b_n \geq 0$ and then the vectors $\{\mathbf{u}^m\}$ satisfy the S -orthogonality

$$(\mathbf{u}^n, \mathbf{u}^m)_S = \delta_{nm}. \quad (57)$$

This process we call the generalized Lanczos (G-Lanczos) process (method). It is well-known that the orthogonality relation is broken for larger n in the Lanczos method and this is also the case here. We adopt the *modified Gram-Schmidt* reorthogonalization process in order to keep the S -orthogonality. (See the results without the *modified Gram-Schmidt* reorthogonalization process in Appendix A.)

We then stop the Lanczos process up to $n = N$ and assume $\mathbf{u}^m = 0$ ($m = N + 1, N + 2, \dots$). This procedure constructs the Krylov subspace

$$K_N(\mathcal{H}, \mathbf{b}) = (\mathbf{b}, \mathcal{H}\mathbf{b}, \mathcal{H}^2\mathbf{b}, \dots, \mathcal{H}^N\mathbf{b}) \quad (58)$$

and the matrix \mathcal{H} is transformed in this subspace to a matrix of a tridiagonal form.

Starting with a natural basis $\mathbf{u}^0 = \mathbf{e}_{j_0}$, one generates vectors \mathbf{u}^n in the Krylov subspace and each vector corresponds to orthonormalized linear combination of atomic orbitals (LCAO);

$$\mathbf{u}^m \Rightarrow \varphi^m(\mathbf{r}) = \sum_j \phi_j(\mathbf{r})u_j^m. \quad (59)$$

The normalized eigen-states in the generated Krylov subspace is denoted by

$$\psi^\alpha(\mathbf{r}) = \sum_{n=0}^N \varphi^n(\mathbf{r})Q_n^{(\alpha)} = \sum_j \phi_j(\mathbf{r})w_j^\alpha, \quad (60)$$

which satisfies the Schrödinger equation

$$\sum_m \mathcal{H}_{nm}Q_m^{(\alpha)} = \varepsilon_\alpha Q_n^{(\alpha)}, \quad (61)$$

where $\mathcal{H}_{nm} = (\mathbf{u}^n, \mathcal{H}\mathbf{u}^m)_S = (\mathbf{u}^n)^t \mathcal{H}\mathbf{u}^m$.

B. Numerical test with NRL Hamiltonian for fcc Au

Chemical potential μ can be evaluated by using Eqs. (21)~(23) in the generalized Lanczos method. Calculation of the Green's function uses Eq.(13) having a

double summation of atomic sites and orbitals and it consumes a long CPU time. On the contrary, the calculation of the density of states by Eq. (14) costs less CPU time. The computational efficiency will be discussed later in Section VI. Here in this subsection, we show several evaluated values, the density of states, the integrated density of states as functions of energies for a system of gold 864 atoms of fcc structure described by the tight-binding Hamiltonian constructed by Mehl and Papaconstantopolous.²⁴

Several evaluated values and consistency between them are summarized in Table I. The parameters in the generalized Lanczos method are $N = 50$, the convergence criterion $\delta = 10^{-6}\text{Ry}$ in the inner CG process of $\mathbf{r}' = S^{-1}\mathbf{r}$. In GsCOCG, the imaginary small energy $\eta = 10^{-3}\text{Ry}$, the total number of the energy integration mesh-points is 3,000, and the convergence criterion $\delta = 10^{-6}\text{Ry}$ in the inner CG and outer iteration procedures. The difference of the calculated total energy is of the order of $10^{-2} \sim 10^{-3}\text{Ry}$. The scale of the band energy is 1 Ry and the relative error may be of 10^{-3} . The bold numbers in Table I are a set of consistent values in each case

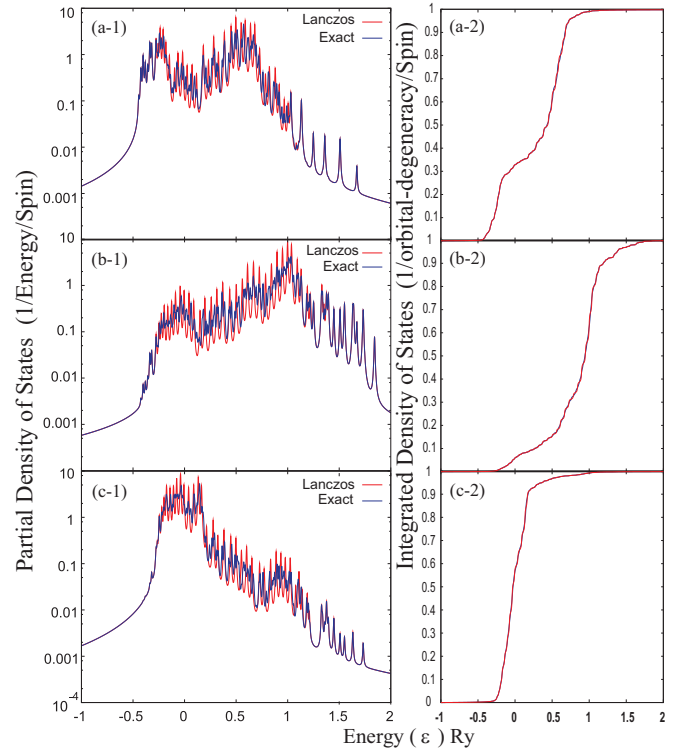


FIG. 4: (Color on line) Partial density of states (pDOS), normalized to unity, and integrated density of states (IDOS) for a system of Au 864 atoms by NRL tight-binding Hamiltonian.²⁴ Comparison is between those of the generalized Lanczos method (red solid lines) and those of the exact ones (blue solid lines). (a-1) and (a-2) :pDOS and IDOS for s-orbitals. (b-1) and (b-2) :pDOS and IDOS for p-orbitals. (c-1) and (c-2) :pDOS and IDOS for d-orbitals. $\eta = 5.0 \times 10^{-3}\text{Ry}$.

TABLE I: The generalized Lanczos process applied to a system of 864 atoms of fcc Au and comparison with that by GsCOCG. The Hamiltonian is the NRL tight-binding form.²⁴ The chemical potential and the total energy are in Ry unit and N_{atom} is the number of atoms in the system.

		G-Lanczos			GsCOCG	
		μ by Eq.(21)	μ by Eq.(22)	μ by Eq.(23)	μ by Eq.(21)	
μ		0.3010 8669	0.2926 6528	0.2870 0985		0.3006 0832
$N_{\text{tot}}/2N_{\text{atom}}$	Eq.(21)	5.5000 0001	5.4809 9705	5.4674 0401	Eq.(21)	5.5000 0000
	Eq.(22)	5.5180 6152	5.4999 9998	5.4865 0739		—
	Eq.(23)	5.5316 2252	5.5135 2184	5.4999 9999		—
$E_{\text{tot}}/2N_{\text{atom}}$	Eq.(26)	-0.1436 6686	-0.1492 6754	-0.1531 8294	Eq.(26)	-0.1436 4084
	Eq.(27)	ρ by Eq.(17)	-0.1311 6499	-0.1364 7104	ρ by Eq.(38)	-0.1251 7255
		ρ by Eq.(18)	-0.1316 2401	-0.1369 4155		
	Eq.(28)	π by Eq.(19)	-0.1311 6490	-0.1364 7094	π by Eq.(39)	-0.1436 4084
		π by Eq.(20)	-0.1316 2391	-0.1369 4146		

(for each equation determining the chemical potential) and the combination of Eqs. (17) and (19), and that of Eqs. (18) and (20) are consistent pairs of data. This consistency between the density matrix and energy density matrix is crucial for consistency between the total energy and force (Appendix B).

In GsCOCG method, calculation of Eqs. (38) and (39) needs ε -integration of $\rho_{ij}(\varepsilon)$ and the numerical integration causes a certain error in the integration of the tail of the spectra. Once we reduce the value of η and increase the ε -points of the integration, this discrepancy can be reduced. In the generalized Lanczos method, the combination of Eqs. (23), (18) and (20) is the best scheme, since we do not use the numerical energy integral.

Figure 4 shows the partial density of states and integrated density of states for s-, p-, and d-orbitals. Those by the generalized Lanczos method are compared with exact results. The peak positions and the tails overlap excellently and we can conclude that the generalized Lanczos method can be powerful and convenient tool. One must notice that the exact results are more smooth in the central energy region, since the correct density of states is more dense in this energy region. In other words, the exact results reserve entire profile with 864×9 peaks but, on the contrary, those by the generalized Lanczos method reserve the profiles with $51 (= N + 1)$ peaks or the density of states is expressed as a polynomial function of energy of the order 51 in the present calculation.

V. GENERALIZED ARNOLDI PROCESS AND DENSITY OF STATES

A. Generalized Arnoldi process

We can construct the Krylov subspace, starting with a natural basis $\mathbf{u}^0 = \mathbf{e}_{j_0}$, by using the Hamiltonian matrix

H , as^{19,27}

$$\mathbf{l}^{n+1} = H\mathbf{u}^n \quad (62)$$

$$\mathbf{k}^{n+1} = \mathbf{l}^{n+1} - \sum_{m=0}^n \mathbf{u}^m (\mathbf{u}^m, \mathbf{l}^{n+1})_S \quad (63)$$

$$\mathbf{u}^{n+1} = \frac{\mathbf{k}^{n+1}}{(\mathbf{k}^{n+1}, \mathbf{k}^{n+1})_S^{1/2}}. \quad (64)$$

This is the Arnoldi process and we call it the generalized Arnoldi (G-Arnoldi) method. The generalized Arnoldi method generates the Krylov subspace

$$\begin{aligned} K_{N+1}(H; \mathbf{b}) &= \text{Span}\{\mathbf{b}, H\mathbf{b}, H^2\mathbf{b}, \dots, H^N\mathbf{b}\} \\ &= \text{Span}\{\mathbf{u}^0, \mathbf{u}^1, \mathbf{u}^2, \dots, \mathbf{u}^N\}. \end{aligned} \quad (65)$$

The generated vector \mathbf{u}^m corresponds to orthonormalized LCAO

$$\varphi^m(\mathbf{r}) = \sum_j \phi_j(\mathbf{r}) u_j^m \quad (66)$$

as in G-Lanczos method. An eigen-function $\psi^\alpha(\mathbf{r}) = \sum_n \varphi^n(\mathbf{r}) Q_n^{(\alpha)}$ satisfies the Schrödinger equation

$$\sum_m \tilde{H}_{nm} Q_m^{(\alpha)} = \varepsilon_\alpha Q_n^{(\alpha)} \quad (67)$$

where $\tilde{H}_{mn} = \langle \varphi^m | \hat{H} | \varphi^n \rangle = (\mathbf{u}^m)^t H \mathbf{u}^n$ and \tilde{H} is an upper Hessenberg matrix. We can say that this procedure is a kind of generalization of the subspace diagonalization of the Krylov subspace developed before.¹³

B. Numerical test with NRL Hamiltonian for fcc Au

We summarize, in Table II, several evaluated values and consistency between them, in comparison with the results of GsCOCG. The system is of 864 atoms of fcc Au by NRL tight-binding Hamiltonian.²⁴ The bold numbers in the table are a set of consistent results in each calculation of the chemical potential. $N = 50$ for the generalized

TABLE II: The generalized Arnoldi process applied to a system of 864 atoms of fcc Au and comparison with that by GsCOCG. The Hamiltonian is the NRL tight-binding form.²⁴ The chemical potential and the total energy are in Ry unit and N_{atom} is the number of atoms in the system.

		G-Arnoldi			GsCOCG			
		μ by Eq.(21)	μ by Eq.(22)	μ by Eq.(23)	μ by Eq.(21)			
μ		0.3039 0679	0.2928 7198	0.2864 6136		0.3006 0832		
$N_{\text{tot}}/2N_{\text{atom}}$	Eq.(21)	5.5000 0002	5.4797 1790	5.4658 1773	Eq.(21)	5.5000 0000		
	Eq.(22)	5.5176 0887	5.5000 0001	5.4865 0981		—		
	Eq.(23)	5.5311 6653	5.5135 1949	5.4999 9999		—		
$E_{\text{tot}}/2N_{\text{atom}}$	Eq.(26)	-0.1423 0073	-0.1482 6563	-0.1522 3179	Eq.(26)	-0.1436 4084		
	Eq.(27)	ρ by Eq.(17)	-0.1300 1076	-0.1351 4434	-0.1389 5498	ρ by Eq.(38)	-0.1251 7255	
		ρ by Eq.(18)	-0.1304 6635	-0.1356 1105	-0.1394 2996			
		Eq.(28)	π by Eq.(19)	-0.1300 1076	-0.1351 4434	-0.1389 5498	π by Eq.(39)	-0.1436 4084
		π by Eq.(20)	-0.1304 6635	-0.1356 1105	-0.1394 2996			

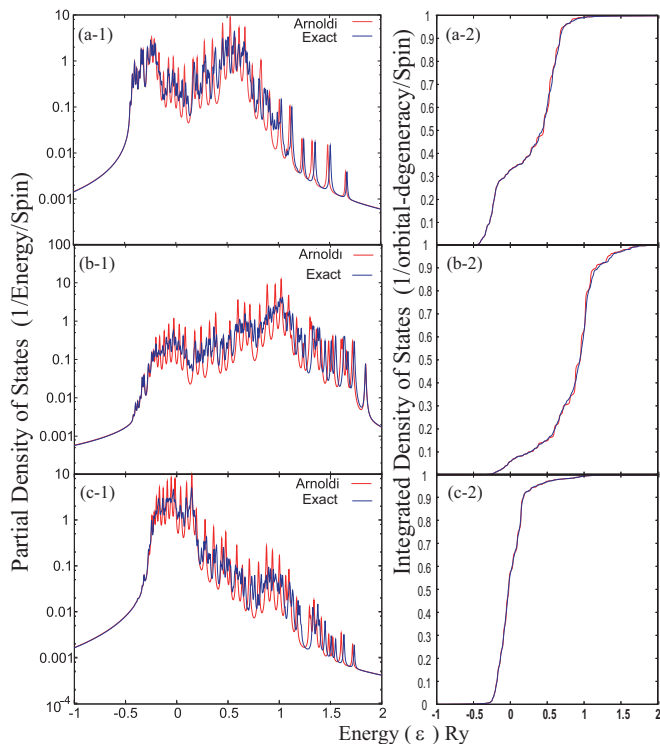


FIG. 5: (Color on line) Partial density of states, normalized to unity, and integrated density of states. Comparison is between those of the generalized Arnoldi method (red solid lines) and those of the exact ones (blue solid lines), for a system of Au 864 atoms by NRL tight-binding Hamiltonian.²⁴ (a-1) and (a-2) :pDOS and IDOS for s-orbitals. (b-1) and (b-2) :pDOS and IDOS for p-orbitals. (c-1) and (c-2) :pDOS and IDOS for d-orbitals. $\eta = 5.0 \times 10^{-3}$ Ry.

Arnoldi process. Data of GsCOCG are the same as in Table I. The calculated values of the total energies agree with those by the generalized Lanczos method and the overall difference is less than 1% as shown in Tables I.

Figure 5 shows the partial density of states and the integrated density of states as functions of energies. The peak positions are deviated slightly from those by the

exact calculation, which one could make smaller with increasing a dimension N of the Krylov subspace.

VI. COMPARISON AMONG GSCOCG, G-LANCZOS METHOD AND G-ARNOLDI METHOD

A. Convergence

The dimension of the Krylov subspace in GsCOCG, G-Lanczos or G-Arnoldi methods equals to $N + 1$ where N is the maximum iteration step. GsCOCG method is very accurate method if one achieves the iteration to have enough small residual norm (e.g. $\delta = 10^{-6}$ Ry). In Fig.2, we have shown the convergence behavior of the residual norms with different seed energies and until much smaller convergence region. One should use the same iteration criteria both in the inner CG and outer procedures in GsCOCG method. It sometimes happens that the resultant DOS shows an un-physical behavior, e.g. negative values of DOS, if one stops the iteration steps before enough convergence in GsCOCG method. On the other hand, G-Lanczos and G-Arnoldi methods never give such un-physical DOS even if one stops at small iteration step because of the expression of Eq.(13). Furthermore, the first N moments are preserved correctly in the energy spectra of G-Lanczos method. In the spectrum of the present model by the exact calculation, we observe about forty prominent peaks and then we use $N = 50$ in the calculations of G-Lanczos and G-Arnoldi procedures. This is presumably the reason why the peak positions and detailed profiles in the spectra of G-Lanczos method show excellent agreement with those of the exact calculation. G-Lanczos method needs the Gram-Schmidt reorthogonalization and also it is necessary to have enough convergence in the inner CG procedure. G-Arnoldi method does not need such reorthogonalization procedure since one solve the eigen-value problem in that subspace.

In condensed matters, the width of the valence and/or conduction bands W may be of the order of 1Ry. Then, when the number of atoms is N_{atom} , we can estimate

TABLE III: Chemical potential and the total energy (in Ry unit) of systems of 864 and 256 atoms of fcc Au²⁴ by three different method. The values of ρ in the G-Lanczos and G-Arnoldi methods are evaluated by Eq.(18).

G-Lanczos		(864 atoms)	(256 atoms)
μ	Eq.(22)	0.2926 6528	0.2875 4133
$E_{\text{tot}}/2N_{\text{atom}}$	Eq.(27)	-0.1364 7104	-0.1358 7639
G-Arnoldi		(864 atoms)	(256 atoms)
μ	Eq.(22)	0.2928 7198	0.2886 2149
$E_{\text{tot}}/2N_{\text{atom}}$	Eq.(27)	-0.1351 4434	-0.1346 6195
GsCOCG		(864 atoms)	(256 atoms)
μ	Eq.(21)	0.3006 0832	0.2947 1535
$E_{\text{tot}}/2N_{\text{atom}}$	Eq.(26)	-0.1436 4084	-0.1433 1925

the separation of each energy level as of the order of $W/(9 \times N_{\text{atom}})$. Presumably 10% of this separation would be an enough accuracy in the energy scale. In our present case, with $N_{\text{atom}} \approx 1,000$, the convergence criterion can be chosen as $0.1 \times W/(9 \times N_{\text{atom}}) \approx 0.1 \times 1/9,000 \approx 10^{-5}\text{Ry}$. We also observed that the maximum iteration steps are almost the same for the convergence criterion $\delta = 10^{-5}$ and $\delta = 10^{-6}$ in GsCOCG and G-Lanczos methods. This is the reason why we choose $\delta = 10^{-6}\text{Ry}$.

We compare the results of the chemical potential and the total band energy of systems of 256 and 864 atoms in Table III. The difference of the chemical potential μ is of the order of 10^{-3}Ry , and that of the total band energy E_{tot} is of the order of 10^{-4}Ry . The level separation in 256 atom system can be estimated as $1.0/(9 \times 256) \approx 4 \times 10^{-4}\text{Ry}$ and that in 864 atom system 10^{-4}Ry . The difference in the chemical potential of two systems of different sizes is due to the difference of total number of levels which changes the value of the chemical potential sensitively. On the other hand, the difference of E_{tot} is just the quantity related to the overall spectrum and we can see an excellent convergence of the results of $N = 50$.

Figure 6 shows the actual convergence behavior of IDOS by G-Lanczos and G-Arnoldi method. The agreement between the results by G-Lanczos or G-Arnoldi methods and those by the exact calculation is excellent both for systems of 864 atoms and that of 256 if we adopt $N = 50$. The most apparent difference appears in the IDOS curves of exact calculation of systems of 256 atoms and 865 atoms in the mid energy region, and the calculated results by our present methods present this difference with complete fidelity.

B. CPU times

We summarize, in Tables IV, the CPU times (by using single CPU of the standard workstation) for (s-orbitals) D_{ii} of the generalized Lanczos and the generalized Arnoldi methods with Eq.(14), that of GsCOCG with Eq.(37), and that of the exact diagonalization

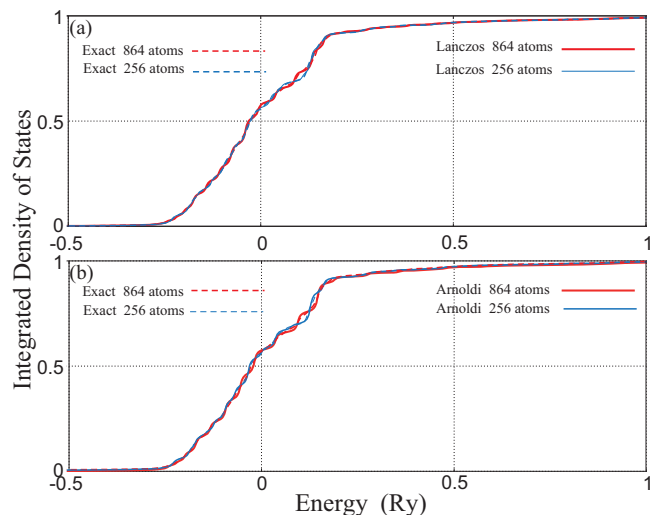


FIG. 6: (Color on line) Comparison of IDOS of d-orbitals for systems of Au 256 and 864 atoms by NRL tight-binding Hamiltonian.²⁴ (a) G-Lanczos (solid line) and exact calculation (chain line) for 864 atoms (red) and 256 (blue) atoms. (b) G-Arnoldi (solid line) and exact calculation (chain line) for 864 atoms (red) and 256 (blue) atoms. The agreement between the results by G-Lanczos or G-Arnoldi methods and those by the exact calculation is excellent.

method for the NRL Hamiltonian of fcc Au system of 256 and 864 atoms.²⁴ The total number of orbitals equals to nine times of the total number of atoms (1 s, 3 p's and 5 d's). We use, in the inner CG process of the generalized Lanczos (G-Lanczos) method, the convergence criterion $\delta = 10^{-6}\text{Ry}$. Two numbers in the row of the CPU time are referred to those of $N = 50$ and $N = 100$, respectively, for G-Lanczos and G-Arnoldi methods, though the results of $N = 100$ almost coincide with those of $N = 50$. For GsCOCG (with shifted 3,000 energy points), the data shown here are those of $\delta = 10^{-6}\text{Ry}$ both for in the inner and outer iteration processes. The repeated time of the inner CG process ($S^{-1}\mathbf{x}$ part) in GsCOCG and G-Lanczos method is $10 \sim 11$. (Repeated time of $25 \sim 27$ is needed for $\delta = 10^{-18}\text{Ry}$.)

The system size dependence of the CPU time is linear for the generalized Arnoldi (G-Arnoldi) method and the generalized Lanczos (G-Lanczos) method, bilinear for GsCOCG method and cubic for the exact calculation. The generalized Arnoldi method is extremely efficient in electronic structure calculations of extra-large systems with several hundred thousands atoms.

C. Applicability to large-scale electronic structure calculations and MD simulations

In the exact calculation and GsCOCG method, calculations of physical properties, such as the density matrix, the energy density matrix, and chemical potential,

TABLE IV: CPU times by using a standard single CPU workstation, for (a) a system of gold 256 atoms (Au256) and (b) gold 864 atoms (Au864) by NRL tight-binding Hamiltonian.²⁴

(a) Au 256		CPU-times (s)		
G-Arnoldi	main part	0.52	1.11	—
	total	1.59	3.20	—
G-Lanczos	inner CG	2.04	3.89	—
	main part	2.89	5.60	—
	total	3.92	7.62	—
GsCOCG	seed	—	—	13.67
	shifted	—	—	7.53
	total	—	—	21.20
Exact		—	—	57.60

(b) Au 864		CPU-times (s)		
G-Arnoldi	main part	1.94	3.76	—
	total	3.00	6.00	—
G-Lanczos	inner CG	7.93	15.13	—
	main part	10.87	21.13	—
	total	11.93	23.31	—
GsCOCG	seed	—	—	140.89
	shifted	—	—	108.36
	total	—	—	249.15
Exact		—	—	2111.51

require the numerical integration as in Eqs. (21), (26), (38) and (39). Therefore, in order to keep high accuracy, the integration needs fine energy mesh points. On the other hand, the generalized Lanczos or the generalized Arnoldi methods use the simple summation of the eigen-states in the mapped subspace in Eqs. (22), (23), and (17) ~ (20). These two methods do not consume the CPU time and give stable values of the density matrix and the energy density matrix.

The CPU times per one MD-step are, for the present models, a few seconds by the generalized Lanczos method and the generalized Arnoldi method. From the above comparison among various viewpoints, we can conclude that the generalized Lanczos method or the generalized Arnoldi method are very suitable to large-scale electronic structure calculations and MD simulation of several tens of thousands atoms and a long MD-steps. On the other hand, GsCOCG method can give excellently rigorous results with more CPU times and may be applicable to problems of a fixed atomic configuration (but not for the MD simulation).

GsCOCG method is based on the three-term recursive equations and we need store three generated vectors at each recursive process. Of course, when the size of the Hamiltonian and overlap matrices are extremely large and the memory size becomes a serious obstacle, (though much smaller consumption than the exact diagonalization method,) we should invent other method of much faster convergence and smaller cost of memory size.

The convergence criterion $\delta = 10^{-5}$ might corresponds to the range of neighboring 1,000 atoms, as already dis-

cussed, and we do not observe any clear difference between results by the present methods and the exact calculations. Even when we should discuss some physics of nano-scale systems, the electronic structure is determined by some nearby surroundings. This idea we call *near-sitedness*.²⁸ Even when we have to deal with a much larger systems, we can use smaller interaction range than the system size due to the near-sitedness. Presumably more serious problem of the system size in some specific problems, for examples, *entire* calculation of nano-device or the electron-strain field interaction such as fracture propagation^{1,2} and dislocation.²⁹

VII. CONCLUSION

We have derived several efficient and accurate algebraic methods to calculate the Green's functions, total/partial density of states and total band energy in case of non-orthogonal atomic orbitals. The method is very general.

We have investigated the accuracy and efficiency by showing numerical data with different numerical procedures. GsCOCG is very accurate with less consumption than the exact diagonalization but may not be appropriate for long MD-step simulations. The generalized Lanczos method becomes applicable to actual large systems with the modified Gram-Schmidt reorthogonalization to maintain the orthogonality of generated basis vectors. Then, the generalized Arnoldi method and the generalized Lanczos method are accurate and efficient, and their CPU times depend linearly upon the system size. Therefore, these two methods would be the most suitable to the large-scale electronic structure calculations and MD simulations. A crucial point we should point out finally is the fact that G-Lanczos and G-Arnoldi methods do not adopt any numerical integration in energy which leads additional numerical error.

Acknowledgments

One of authors (T. Fujiwara) expresses sincere thanks to TOYOTA Motor Corporation for the financial support. Numerical calculation was partly carried out using the supercomputer facilities of the Institute for Solid State Physics, University of Tokyo. Our research progress of large-scale systems and other information can be found on the WEB page of ELSEES (Extra-Large Scale Electronic Structure calculation) Consortium; <http://www.elses.jp>.

Appendix A: Re-orthogonalization by modified Gram-Schmidt method

The three-term recursive relation in the generalized Lanczos method guarantees theoretically the automatic

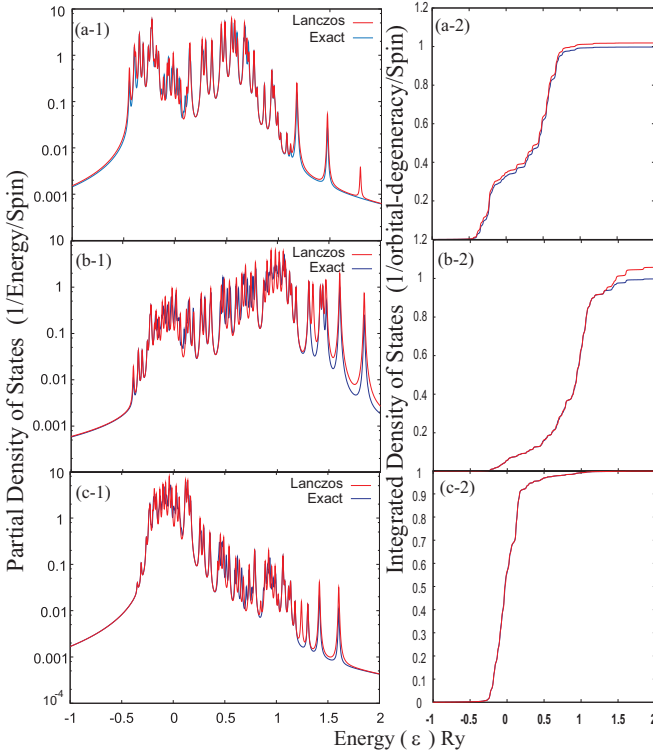


FIG. 7: (Color on line) Partial density of states and integrated ones without the modified Gram-Schmidt reorthogonalization of the generalized Lanczos method (red solid lines) and those by the exact ones (blue solid lines) for a system of Au 256 atoms by NRL tight-binding Hamiltonian.²⁴ $N = 50$. (a-1) and (a-2) :pDOS and IDOS for s-orbitals. (b-1) and (b-2) :pDOS and IDOS for p-orbitals. (c-1) and (c-2) :pDOS and IDOS for d-orbitals. One should notice that the normalization of the integrated density of states is broken without reorthogonalization procedure and that some “ghost” peaks appear due to incorrect mixing of states. $\eta = 5.0 \times 10^{-3}$ Ry.

S-orthogonalization. However, the orthogonality is broken in the numerical calculation procedure. This problem causes several troubles such as the existence of constant background of error in the spectrum,¹⁴ appearance of “ghost” structure in spectrum due to erroneous mix-

ing of states and a broken normalization of the partial density of states.

Figure 7 shows the examples of this broken orthonormality, in a system of 256 atoms of fcc Au by using the NRL Hamiltonian. One can see the “ghost” peaks (e.g. at $\varepsilon \simeq 1.8$ Ry in (a-1), at $\varepsilon \simeq 1.25 \sim 1.3$ Ry in (b-1) and (c-1)) and broken normalization (e.g. in (a-2) and (b-2)). These problems are solved by the re-orthogonalization with the modified Gram-Schmidt method.

Appendix B: Consistency between the total energy minimum and a vanishing force

We should construct our eigen-states in a small subspace and a certain numerical error is unavoidable in evaluated total energy and force. Even in that case, the consistency between the total band energy minimization and a vanishing atomic force is the most important in the electronic structure calculation in equilibrium atom configuration. In the framework of the tight-binding model, the force (due to band energy) acting on an atom I is evaluated by a formula

$$\mathbf{F}_I = -2 \sum_{ij} \left(\rho_{ij} \frac{\partial H_{ij}}{\partial \mathbf{R}_I} - \pi_{ij} \frac{\partial S_{ij}}{\partial \mathbf{R}_I} \right), \quad (\text{B1})$$

which can be rewritten, with only an assumption of the eigen-state property Eq.(8) in the mapped subspace, as

$$\mathbf{F}_I = -2 \frac{\partial}{\partial \mathbf{R}_I} \left\{ \sum_{ij} (\rho_{ij} H_{ij}) - \sum_{ij} (\pi_{ij} S_{ij}) \right\} - \frac{\partial}{\partial \mathbf{R}_I} \sum_{\alpha} f(\varepsilon_{\alpha}) \varepsilon_{\alpha}. \quad (\text{B2})$$

Therefore, calculated atomic and electronic configuration of the minimum total energy is consistent with that of vanishing atomic force, if the identity $\sum_{ij} (\rho_{ij} H_{ij}) = \sum_{ij} (\pi_{ij} S_{ij})$ is satisfied always in any atomic configuration. It should be noticed that the above equality is satisfied in the mapped subspace as described in IIC 2. It is important in actual calculating procedure that we should use the consistent pair of equations as Eqs. (17) and (19) or Eqs. (18) and (20).

* Present address: Institute of Mechanics, Chinese Academy of Sciences, Beijing, China

† Corresponding author: fujiwara@coral.t.u-tokyo.ac.jp

¹ T. Hoshi and T. Fujiwara, J. Phys. Soc. Jpn. **72**, 2429 (2003).

² T. Hoshi, Y. Iguchi and T. Fujiwara, Phys. Rev. B **72**, 075323 (2005).

³ Y. Iguchi, T. Hoshi and T. Fujiwara, Phys. Rev. Lett. **99**, 125507 (2007).

⁴ T. Hoshi and T. Fujiwara, J. Phys. Condensed Matters **21**, 272201 (2009).

⁵ S. Goedecker, Rev. Mod. Phys. **71**, 1085 (1999)

⁶ S. Goedecker and L. Colombo, Phys. Rev. Lett. **73**, 122 (1994).

⁷ W. Yang, Phys. Rev. Lett. **66**, 1438 (1991); T. Ozaki, Phys. Rev. B **74**, 245101 (2006).

⁸ X.-P. Li, R. W. Nunes, and D. Vanderbilt, Phys. Rev. B **47**, 10891 (1993).

⁹ F. Mauri, G. Galli, and R. Car, Phys. Rev. B **47**, 9973 (1993).

¹⁰ C.-K. Skylaris, P. D. Haynes, A. A. Mostofi, and M. C. Payne, J. Chem. Phys. **122**, 084119 (2005).

¹¹ J. M. Soler, E. Artacho, J. D. Gale, A. García, J. Junquera, P. Ordejón, and D. Sánchez-Portal, J. Phys. Con-

- dens. Matter **14**, 2745 (2002).
- ¹² P. Ordejón, *Comp. Mat. Sci.* **12**, 157 (1998).
- ¹³ R. Takayama, T. Hoshi and T. Fujiwara, *J. Phys. Soc. Jpn.* **73**, 1519 (2004).
- ¹⁴ R. Takayama, T. Hoshi, T. Sogabe, S-L. Zhang and T. Fujiwara, *Phys. Rev. B* **73**, 165108 (2006).
- ¹⁵ T. Sogabe, T. Hoshi, S.-L. Zhang, and T. Fujiwara, *Electronic Transactions on Numerical Analysis (ETNA)*, **31**, 126 (2008).
- ¹⁶ T. Sogabe, T. Hoshi, S.-L. Zhang, and T. Fujiwara, *Frontiers of Computational Science*, pp. 189-195, Ed. Y. Kaneda, H. Kawamura and M. Sasai, (Springer Verlag, Berlin Heidelberg, 2007).
- ¹⁷ C. Lanczos, *J. Res. Natl Bur. Stand.* **45**, 225 (1950); C. Lanczos, *J. Res. Natl Bur. Stand.* **49** 33 (1952).
- ¹⁸ R. Haydock, *Solid State Physics* **35** pp.225-228, Ed. H. Ehrenreich, F. Seitz, and D. Turnbull (Academic Press, New York, 1980).
- ¹⁹ *Templates for the Solution of Algebraic Eigenvalue Problems*, Chapter 5, Edited by Z. Bai, J. Demmel, J. Dongarra, A. Ruhe, and H. van der Vorst, (SIAM, Philadelphia, 2000).
- ²⁰ M. Elstner, D. Porezag, G. Jungnickel, J. Elsner, M. Haugk, Th. Frauenheim, S. Suhai and G. Seifert, *Phys. Rev. B* **58**, 7260 (1998).
- ²¹ T. Fujiwara, T. Hoshi, and S. Yamamoto, *J. Phys.: Condens. Matter* **20**, 294202 (2008).
- ²² T. Sogabe and S.-L. Zhang, talk in the International Conference *Numerical Analysis and Scientific Computing with Applications*, Agadir, Morocco, May 18-22, 2009; in preparation, T. Sogabe, T. Hoshi, S.-L. Zhang and T. Fujiwara, *Solution of Generalized Shifted Linear Systems with Complex Symmetric Matrices*.
- ²³ A. Frommer, *Computing* **70**, 87 (2003).
- ²⁴ M. J. Mehl and D. A. Papaconstantopoulos, *Phys. Rev. B* **54**, 4519 (1996); F. Kirchhoff, M. J. Mehl, N. I. Papanicolaou, D. A. Papaconstantopoulos, and F. S. Khan, *Phys. Rev. B* **63**, 195101 (2001).
- ²⁵ S. Yamamoto, T. Sogabe, T. Hoshi, S.-L. Zhang, and T. Fujiwara, *J. Phys. Soc. Jpn* **77**, 114713 (2008).
- ²⁶ T. Ozaki and K. Terakura, *Phys. Rev. B* **64**, 195126 (2001).
- ²⁷ T. Hoshi, T. Fujiwara, S. Nishino, S. Yamamoto, Y. Zempo, M. Ishida, T. Sogabe, and S.-L. Zhang, in preparation.
- ²⁸ W. Kohn, *Phys. Rev. Lett.* **76**, 3168 (1996).
- ²⁹ M. Miyata and T. Fujiwara, *Phys. Rev. B* **63**, 045206 (2001).